

# Brain-grounding of semantic vectors improves neural decoding of visual stimuli

Shirin Vafaei<sup>1</sup>, Ryohei Fukuma<sup>1,2,3</sup>, Huixiang Yang<sup>2</sup>, Haruhiko Kishima<sup>1</sup>, \*Takufumi Yanagisawa<sup>1,2,3</sup>

<sup>1</sup>Department of Neurosurgery, Graduate School of Medicine, Osaka University, Suita, Japan

<sup>2</sup>Institute for Advanced Co-Creation Studies, Osaka University, Suita, Japan

<sup>3</sup>ATR Computational Neuroscience Laboratories, Seika-cho, Japan

\*Corresponding author: Takufumi Yanagisawa (tyanagisawa@nsurg.med.osaka-u.ac.jp)

## Keywords

Brain decoding, representation learning

## Abstract

Developing algorithms for accurate neural decoding of mental contents is a long-cherished goal in the field of neuroscience. Brain decoding is typically employed by training machine learning models to map neural data into a pretrained feature vector representation of stimuli. These vectors are usually driven from image-based and/or text-based feature spaces. This implies that their intrinsic characteristics might be fundamentally different than those encoded in neural activity patterns, resulting in limiting the capability of brain decoders to accurately learn this mapping. To address this issue, we propose a representation learning framework, termed brain-grounding of semantic vectors, that fine-tunes pretrained feature vectors to better align with the structure of neural representation of visual stimuli in the human brain. We trained this model with functional magnetic resonance imaging (fMRI) of 150 visual stimuli categories and then performed zero-shot brain decoding on 1) fMRI, 2) magnetoencephalography (MEG), and 3) electrocorticography (ECoG) neural data of visual stimuli. Our results demonstrated that by using the fMRI-based brain-grounded vectors, the zero-shot decoding accuracy of brain data from all three neuroimaging modalities increases. These findings underscore the potential of incorporating a richer array of brain-derived features to enhance the performance of brain decoding algorithms.

## Introduction

The development of brain decoding algorithms is essential for advancing Brain-Machine Interfaces (BMIs)<sup>1-4</sup> enabling precise communication and motor control for individuals with speech or motor impairments. Simultaneously, these algorithms offer a unique opportunity to delve into the intricate processes of human brain information processing<sup>5-10</sup>, shedding light on the fundamental mechanisms that underlie information encoding process in the human brain. Furthermore, this progress can augment the effectiveness of neurofeedback systems by enabling the precise decoding of cognitive patterns and delivering real-time neurofeedback, thereby assisting patients in the refinement of their cognitive and emotional faculties<sup>11-14</sup>.

Previous studies have shown that neural activity patterns can be decoded to reveal *information* about perceived or imagined visual stimuli (i.e., images). This *information* can take the form of semantic attributes<sup>10,15–18</sup>, category-level classes<sup>5,7,15,19,20</sup> or even as reconstructed visual representations of the images<sup>21–24</sup>. Decoding typically involves representing the desired attribute as a pretrained feature vector, often derived from object recognition neural networks<sup>15,25</sup>, multimodal models<sup>26,27</sup> or word co-occurrence statistics<sup>12,28–30</sup>. Afterwards, machine learning models are trained to map neural activity patterns to these corresponding feature vectors.

While pretrained feature vectors have enabled brain decoding with an above-chance accuracy, current models still often struggle to accurately learn this mapping. This is particularly evident in zero-shot decoding scenarios, where decoders must generalize to novel categories not encountered during training<sup>31</sup>. Given the impracticality of training decoders on all possible semantic categories, there is a pressing need for more robust and flexible decoding models.

In this study, we hypothesized that if the vectors used to represent the stimuli are more aligned with how visual stimuli are encoded in the human brain, decoders can better learn this mapping, and even generalize to unseen semantic categories based on the information encapsulated within the more brain-aligned vectors.

The key insight to this idea is inspired by recent findings that brain-like or brain-integrated features can improve object recognition<sup>32</sup>, few-shot learning and anomaly detection tasks<sup>33</sup>, or obtaining consistent and high-performing latent spaces by jointly learning from both behavioral and neural data<sup>34</sup>. However, it has remained unclear whether semantic spaces with more brain-aligned representations can lead to more accurate zero-shot brain decoding.

To create a brain-aligned semantic vector representation of stimuli, we propose a framework called "brain-grounding of semantic vectors," which is an autoencoder that reconstructs the pretrained feature vectors while constraining the second-order statistical features of its latent space to become as similar as possible to those of brain activity patterns. The resulting vectors extracted from the latent space of the autoencoder after training are the so-called *brain-grounded semantic vectors*. We investigated whether utilizing brain-grounded semantic vectors could improve zero-shot decoding<sup>15</sup> and identification<sup>15,35</sup> accuracy for 1) brain activity patterns obtained by the same neuroimaging technique used to fine-tune the pretrained feature spaces, and 2) brain activity patterns obtained by a different neuroimaging technique than the one used for fine-tuning.

More particularly, we trained the brain-grounding framework by leveraging the brain activity patterns measured by fMRI and then tested the performance of the zero-shot decoding and identification of resulting brain-grounded vectors on the brain activity data measured by fMRI, MEG and ECoG. This cross-modality

approach is critical because fMRI, MEG and ECoG measure distinct aspects of brain activity: fMRI captures hemodynamic changes (BOLD signals)<sup>36</sup>, ECoG records electrical activity<sup>37</sup>, and MEG detects magnetic fields<sup>38</sup>. Successful generalization across modalities would suggest that our vectors represent fundamental aspects of neural coding that is independent of specific measurement technique.

## Results

### Brain-grounding of semantic vectors

We developed a multimodal learning autoencoder framework that works by taking a pretrained feature space and brain activity patterns corresponding to the visual stimuli dataset and training it to integrate the structure of visual representation in the human brain with the pretrained feature spaces. As for the selection of pretrained feature spaces, we leveraged two different feature spaces. First is an image-based feature space: features from the image encoder model of CLIP<sup>27</sup> and second is a text-based feature space: features from the *Global Vectors for Word Representation* (GloVe) model<sup>30</sup>. The fMRI dataset used here to fine-tune the pretrained feature vectors was the generic object decoding (GOD) dataset<sup>15</sup>, which contains fMRI brain activity patterns of 5 subjects while they were watching 1200 images of 200 distinct object categories selected from ImageNet<sup>39</sup>. The GOD dataset has been uniquely designed to prevent any overlap between the categories used for training and those used for testing. This design makes it a seamless benchmark for assessing the zero-shot prediction capabilities of decoding models, as it ensures these models are evaluated on their ability to generalize to entirely new categories without prior exposure.

First, we extracted the original semantic vectors for each category in the GOD dataset (see methods) and represented each category by its corresponding pretrained feature vector. Then, to obtain the “brain-grounded semantic space”, we trained the autoencoder with a two-term objective function. The first term is a simple mean squared error (MSE) loss between true and predicted pretrained feature vectors (with the goal of reconstructing them). The second term is the MSE loss between the representational similarity matrix (RSM)<sup>34</sup> of fMRI signals and the autoencoder’s latent space in each batch. Mathematically:

$$loss = \frac{1}{m} \sum_{i=1}^m \left[ (\alpha) (y - y')^2 + (1 - \alpha) (RSM_l - RSM_b)^2 \right]$$

(1)

where  $y$  is the original semantic vector,  $y'$  is the reconstructed semantic vector,  $RSM_l$  is the RSM of autoencoder’s hidden layer,  $RSM_b$  is the RSM of corresponding brain activity patterns, and  $m$  is the number of samples in each batch.  $\alpha$  is the hyperparameter that determines the extent of brain-grounding.

Given that our aim here is to decode the visual object categories, we used the fMRI activity patterns of lateral occipital complex (LOC) region of human brain to fine-tune pretrained feature vectors. LOC is a

region that is located in the occipital lobe and is primarily responsible for visual processing of objects and shapes<sup>40</sup>. Concurrently, to choose the appropriate pretrained feature vectors, we extracted the category-specific pretrained feature vectors of each category in the training data of GOD dataset.

For each subject in the GOD dataset, brain region, pretrained feature vector and  $\alpha$ , we trained a different autoencoder. When training the autoencoder for a particular subject (i.e., subject  $A$ ) in the GOD dataset, we used the averaged RSM of fMRI brain signals of all other subjects in the GOD dataset. We later used these brain-grounded vectors for decoding the fMRI brain signals of subject  $A$ , to avoid information leakage. We trained autoencoders on a wide range of  $\alpha$  consisting of values from the [0.0001, 0.001, 0.01, 0.1, 1]. We specially included 1 as one of the options to see if we exclude the brain-grounding part from this framework, how it will affect the downstream analyses. Figure 1 shows an overall procedure of this framework.

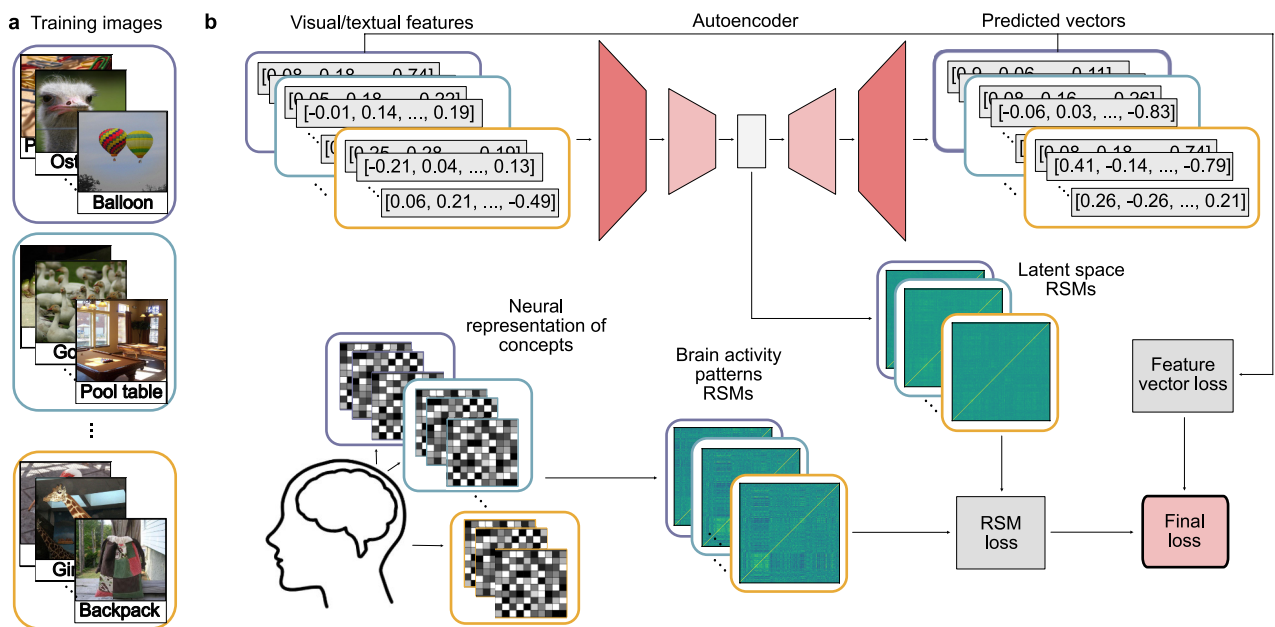


**Figure 1| Samples of the visual stimuli dataset and the brain-grounding framework.** (a) Samples of images in the GOD dataset. Rectangles indicate sample image batches used for training. (b) The brain-grounding framework. First, pretrained visual or textual features are extracted. Then, an autoencoder is trained to reconstruct these features while aligning the representational similarity matrix (RSM) of its latent space with the RSM of corresponding brain activity patterns.

## fMRI brain decoding and identification of visual stimuli

We performed brain decoding and identification for each feature space type and subject separately.

Decoding was conducted by training linear regression models to map brain activity patterns to their corresponding feature vectors. For all samples and each unit in the semantic vectors, a separate set of linear regression models was trained. To comprehensively evaluate decoding accuracy, we employed both sample-wise and dimension-wise correlation metrics. Sample-wise correlation, calculated as the average Pearson correlation between true and predicted vectors across all samples and subjects, provides a global measure of the model's ability to reconstruct entire brain activity patterns<sup>6,7,41,42</sup>. On the other hand, dimension-wise correlation, calculated as the average Pearson correlation across feature units, assesses the model's capacity



to capture fine-grained representational details at the level of individual semantic features<sup>15,17,43,44</sup>. This metric is essential for understanding how well the model decodes specific semantic or conceptual features embedded within the neural representations.

Furthermore, we evaluated the models' identification accuracy, assessing their abilities to correctly classify stimuli based on the predicted feature vectors. This evaluation is critical for determining the practical utility of the decoding models in real-world applications, such as brain-computer interfaces or neurofeedback systems<sup>6,35</sup>. For this purpose, we computed the Pearson correlation coefficient between the predicted semantic vector and all other candidate vectors. The accuracy is defined by the percentage of candidate categories, in which their correlation with the predicted vector were lower than the correlation between the actual true and predicted vector. The final identification accuracy is determined by averaging the identification accuracies across all categories and subjects in the test dataset.

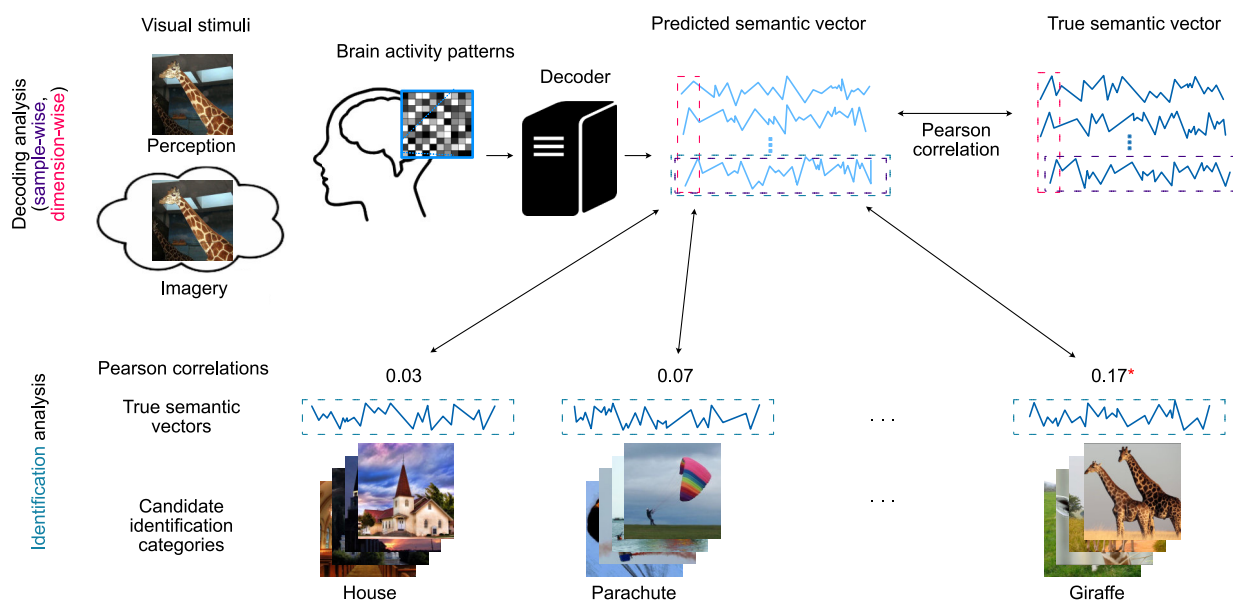


**Figure 2| Decoding and identification procedure.** Brain decoders are trained to map brain activity patterns resultant of a visual stimulus to their corresponding feature vectors. In the identification analysis, a large set of candidate stimuli is considered. The Pearson correlation coefficient is calculated between the predicted semantic vector and the semantic vectors of each candidate stimulus, facilitating identification of the most likely perceived or imagined stimulus.

To evaluate the performance of our decoding and identification methods, we compared them against a chance-level baseline. Specifically, we compared the decoding and identification results obtained from the original data with those obtained from shuffled data. For sample-wise and dimension-wise decoding, shuffled accuracy was determined by correlating predicted feature vectors with randomly shuffled true feature vectors. For identification, shuffled accuracy was obtained by correlating predicted vectors with both shuffled true vector and all other candidate vectors. The shuffled identification accuracy was then defined as the percentage of candidate categories where their correlation with the predicted vector was lower than the correlation between the shuffled true and predicted vectors.

Figure 3 presents the fMRI decoding and identification results for both perception and imagery stimuli, using either CLIP-based or GloVe-based feature vectors. For all analyses (sample-wise decoding, dimension-wise decoding and identification), the real accuracy was significantly higher than the corresponding shuffled accuracy (one-sided t-test after Fisher's z-transform,  $P < 0.05$ ; see Extended Data Tables 1-6 for exact values).

Furthermore, we observed that decoding accuracy changes depending on the level of brain-grounding. Sample-wise decoding accuracy significantly changed for different values of  $\alpha$  in both perception data (CLIP-based feature vectors,  $F_{(5, 24)} = 79.900$ ,  $P < 0.001$ ; GLoVe-based feature vectors,  $F_{(5, 24)} = 321.611$ ,  $P < 0.001$ ; one-way ANOVA, Bonferroni corrected significance level = 0.05/12; Fig. 3a) and imagery data (CLIP-based feature vectors,  $F_{(5, 24)} = 54.716$ ,  $P < 0.001$ ; GLoVe-based feature vectors,  $F_{(5, 24)} = 93.186$ ,  $P < 0.001$ ; one-way ANOVA, Bonferroni corrected significance level = 0.05/12; Fig 3b).

Notably, within the CLIP-based vectors, the decoding accuracies corresponding to the brain-grounded vectors with larger  $\alpha$  values initially decreased (Perception,  $P < 0.01$ , Tukey's HSD post-hoc test, comparison between brain-grounded vectors with  $\alpha = 10^{-1}$  and original feature vectors; Imagery,  $P < 0.05$ , Tukey's HSD post-hoc test, comparison between brain-grounded vectors with  $\alpha = 1$  and original feature vectors and between  $\alpha = 10^{-1}$  and original feature vectors; Fig. 3a, b). However, these accuracies gradually increased as alpha decreased, resulting in brain-grounded vectors with the highest levels of brain information ( $\alpha = 10^{-3}$  and  $\alpha = 10^{-4}$ ) yielded the highest decoding accuracies, significantly exceeding those of the original pretrained feature vectors and brain-grounded vectors with  $\alpha = 1$  ( $P < 0.01$ , Tukey's HSD post-hoc test; Fig. 3a, b). Within the GLoVe-based feature vectors, the decoding accuracies tended to increase while  $\alpha$  was getting smaller and became significantly higher than the decoding accuracy of original feature vectors (Perception,  $P < 0.01$ , Tukey's HSD post-hoc test; Imagery,  $P < 0.01$ , Tukey's HSD post-hoc test; Fig 3a, b). Also, decoding accuracies corresponding to the two top smallest values of alpha ( $\alpha = 10^{-3}$  and  $\alpha = 10^{-4}$ ) significantly increased compared to the brain-grounded vectors with  $\alpha = 1$  (Perception,  $P < 0.01$ , Tukey's HSD post-hoc test; Imagery,  $P < 0.01$ , Tukey's HSD post-hoc test; Fig 3a, b).

Similarly, in dimension-wise results of perception data, the decoding accuracy of brain-grounded vectors significantly changed among different values of  $\alpha$  (CLIP-based feature vectors,  $F_{(5, 24)} = 9.620$ ,  $P < 0.001$ ; GLoVe-based feature vectors,  $F_{(5, 24)} = 5.050$ ,  $P = 0.0027$ ; one-way ANOVA, Bonferroni corrected significance level = 0.05/12; Fig. 3c). More particularly, in the CLIP-based results, the decoding accuracies tended to increase while alpha was getting smaller and become significantly higher than the decoding accuracy of original feature vectors ( $P < 0.05$ , Tukey's HSD post-hoc test; Fig. 3c). concurrently, in the GLoVe-based feature vectors, the decoding accuracies of the two top brain-grounded vectors with the

highest level of brain information ( $\alpha = 10^{-3}$  and  $\alpha = 10^{-4}$ ) significantly increased compared to the decoding accuracy of original feature vectors ( $P < 0.05$ , Tukey's HSD post-hoc test; Fig. 3c). However, dimension-wise decoding accuracy of imagery data did not significantly change for different values of  $\alpha$  (CLIP-based feature vectors,  $F_{(5, 24)} = 0.709$ ,  $P = 0.6224$ ; GLoVe-based feature vectors,  $F_{(5, 24)} = 0.760$ ,  $P = 0.5875$ ; one-way ANOVA, Bonferroni corrected significance level = 0.05/12; Fig. 3d).

Additionally, we observed that for both CLIP-based and GLoVe-based feature vectors, the identification accuracies across different groups of original and brain-grounded vectors did not significantly change for different values of  $\alpha$  (Perception data, CLIP-based feature vectors,  $F_{(5, 24)} = 2.542$ ,  $P = 0.0555$ ; perception data, GLoVe-based feature vectors,  $F_{(5, 24)} = 0.8$ ,  $P = 0.5606$ ; imagery data, CLIP-based feature vectors,  $F_{(5, 24)} = 2.219$ ,  $P = 0.0855$ ; imagery data GLoVe-based feature vectors,  $F_{(5, 24)} = 0.273$ ,  $P = 0.9235$ ; one-way ANOVA, Bonferroni corrected significance level = 0.05/12; Fig. 3e ,f; see Extended Data Table 7 and 8 for exact values).

Moreover, we investigated whether brain-grounding could enhance the category discriminability of each feature unit, defined as the ratio of inter-category to intra-category variation in feature values ( $F$ -statistic)<sup>15</sup>. Since GloVe labels are identical for all images within a category, we focused on calculating category discriminability solely for CLIP-based feature vectors. We computed the category discriminability of each feature unit across 19,933 ImageNet categories, with 8 images per category. The distribution of  $F$ -values for CLIP-based feature vectors showed that  $F$ -values for brain-grounded vectors significantly increases compared to the  $F$ -value of original feature vectors ( $p < 0.001$ ; two-sided Wilcoxon rank-sum test) and  $F$ -values corresponding to the brain-grounded vectors with  $\alpha \leq 10^{-2}$  significantly increases compared to the  $F$ -values of feature vectors with  $\alpha = 1$  ( $p < 0.001$ ; Fig. 3g).

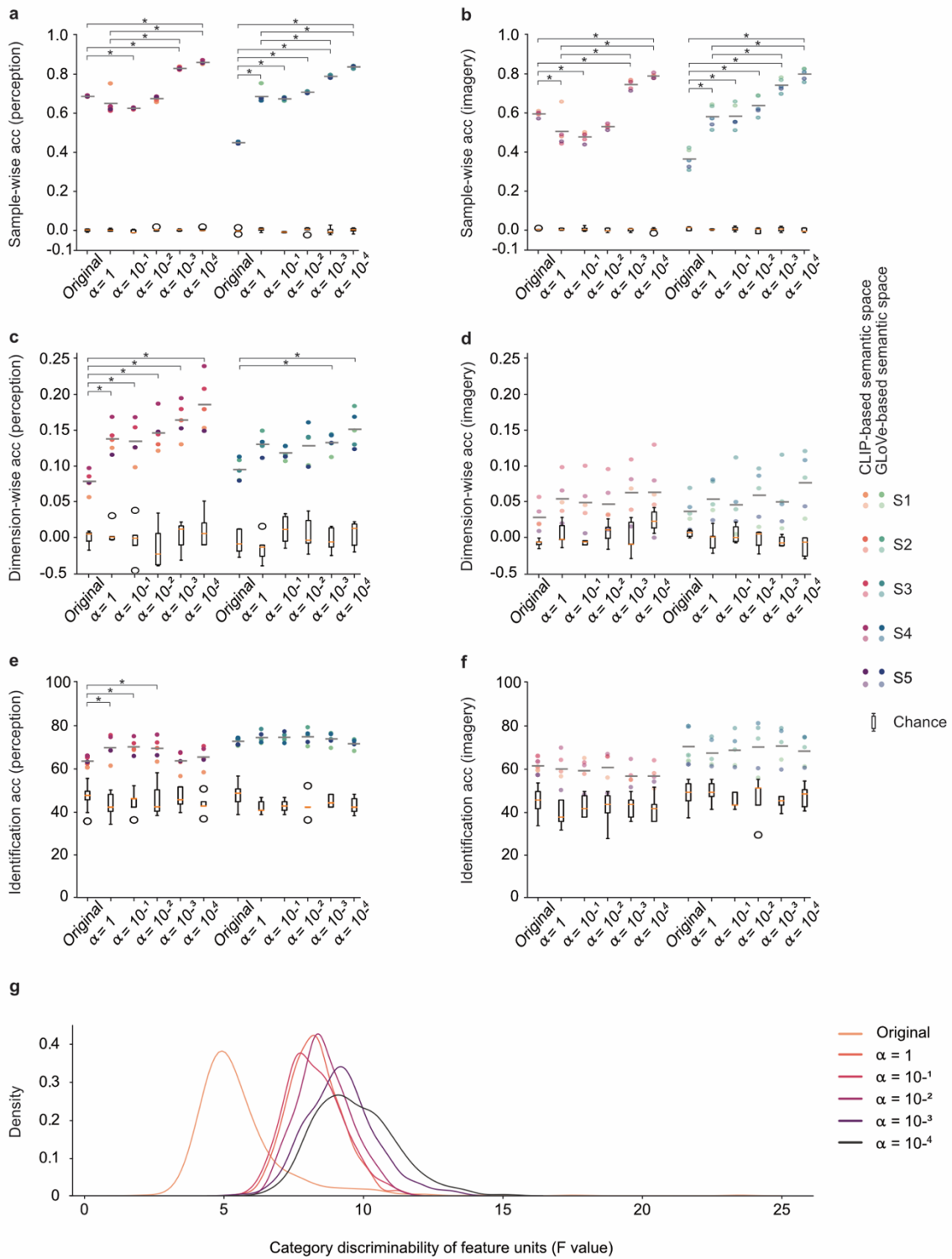


**Figure 3 | fMRI decoding and identification results.** fMRI decoding and identification results of perception and imagery data into the original and brain-grounded feature vectors of CLIP and GloVe, evaluated by (a, b) sample-wise decoding accuracy and (c, d) dimension-wise decoding accuracy, and (e, f) identification accuracy. For clarity, only the significant differences between the brain-grounded vectors with the original pretrained feature vectors and with the brain-grounded vectors with  $\alpha = 1$ , are depicted. For all pairwise significant results, see the supplementary figure 1. (g) Distribution of category discriminability of original and brain-grounded CLIP-based feature vectors.

## Generalization of decoding performance on other modalities: MEG and ECoG datasets

To assess the generalizability of utilizing the fMRI-derived brain-grounded vectors to decoding other types of neuroimaging brain data, we performed decoding and identification analyses on MEG and ECoG neural data from different set of subjects that were exposed to the same visual stimuli. For MEG analyses, we used the source-estimated signals covering the ventral visual stream region of human brain (see methods for source localization and detailed preprocessing procedure). For ECoG, we concatenated the high- $\gamma$  power of brain signals from 4 subjects that had electrodes implanted within their ventral visual cortex, with a total of 231 electrodes (see Methods). We trained separate linear regression models as brain decoders for each of the MEG and ECoG datasets, subjects and feature space types, using fMRI brain-grounded vectors derived from averaging RSM matrices across all 5 fMRI subjects.

Figure 4 shows the decoding and identification results of MEG neural data. Consistent with the fMRI analyses, we first evaluated whether the MEG data can be successfully decoded. In all analyses of MEG data (i.e., sample-wise decoding, dimension-wise decoding and identification), the real decoding accuracy was significantly higher than the corresponding shuffled decoding accuracy ( $P < 0.05$ , one-sided t-test after Fisher's z-transform; see Extended Data Tables 9-11 for exact values; Fig. 4a-c).

Subsequently, we evaluated the effect of using fMRI-based brain-grounded feature vectors for probing whether they can improve the sample-wise and dimension-wise decoding and identification accuracies of MEG neural data. Sample-wise decoding accuracy significantly changed for different values of  $\alpha$  (CLIP-based feature vectors,  $F_{(5, 12)} = 41.587$ ,  $P < 0.001$ ; GLoVe-based feature vectors,  $F_{(5, 12)} = 368.447$ ,  $P < 0.001$ ; one-way ANOVA, Bonferroni corrected significance level = 0.05/12; Fig. 4a). Decoding accuracies of brain-grounded vectors with  $\alpha = 1$  significantly increased compared to the original feature vectors (CLIP-based feature vectors,  $P = 0.034$ ; GLoVe-based feature vectors  $P < 0.0$ ; Tukey's HSD post-hoc test; Fig. 4a). Within the CLIP-based vectors, decoding accuracies corresponding to the brain-grounded vectors with the highest level of brain information ( $\alpha = 10^{-3}$  and  $\alpha = 10^{-4}$ ) became the highest and they became significantly higher than the decoding accuracy of original feature vectors ( $P < 0.01$ , Tukey's HSD post-hoc test; Fig. 4a) and feature vectors with  $\alpha = 1$  ( $P < 0.01$ , Tukey's HSD post-hoc test; Fig. 4a). Within the GLoVe-based vectors, decoding accuracies corresponding to the brain-grounded vectors with  $\alpha \leq 10^{-1}$  started to increase while  $\alpha$  was getting smaller and they became significantly higher than the decoding accuracy of original feature vectors ( $P < 0.01$ , Tukey's HSD post-hoc test; Fig. 4a) and the decoding accuracies corresponding to the brain-grounded vectors with  $\alpha \leq 10^{-2}$  became significantly higher than decoding accuracy corresponding to the vectors with  $\alpha = 1$  ( $P < 0.01$ , Tukey's HSD post-hoc test; Fig. 4a).

In the dimension-wise decoding results of MEG, only decoding accuracies for GLoVe-based feature vectors changed for different values of  $\alpha$  (CLIP-based feature vectors,  $F_{(5, 12)} = 1.392$ ,  $P = 0.2947$ ; GLoVe-based feature vectors,  $F_{(5, 12)} = 4.766$ ,  $P = 0.0125$ ; Fig. 4b). Additionally, the dimension-wise decoding accuracy of the GLoVe-based brain-grounded tended to increase while  $\alpha$  was getting smaller and more particularly,

decoding accuracies corresponding to the feature vectors with  $\alpha = 10^{-1}$ ,  $\alpha = 10^{-2}$  and  $\alpha = 10^{-3}$  significantly increased compared to the dimension-wise decoding accuracy of original GLoVe feature vectors ( $P < 0.05$ , Tukey's HSD post-hoc test ; Fig 4b)

Furthermore, the identification results of MEG data significantly changed for different values of a  $\alpha$  (CLIP-based feature vectors,  $F_{(5, 12)} = 23.130$ ,  $P < 0.001$ ; GLoVe-based feature vectors,  $F_{(5, 12)} = 125.602$ ,  $P < 0.001$ ; Fig 4a). Within the CLIP-based vectors, identification accuracies corresponding to brain-grounded vectors with  $\alpha = 1$  and  $\alpha = 10^{-1}$  decreased compared to the identification accuracy of original feature vectors ( $P < 0.01$ , Tukey's HSD post-hoc test; Fig. 4c), but then identification accuracies corresponding to vectors with higher level of brain information ( $\alpha = 10^{-2}$ ,  $\alpha = 10^{-3}$  and  $\alpha = 10^{-4}$ ) significantly increased compared to the identification accuracies of brain-grounded feature vectors with  $\alpha = 1$  ( $P < 0.01$ , Tukey's HSD post-hoc test; Fig. 4c). Within the GLoVe-based vectors, identification accuracies corresponding to the brain-grounded vectors with  $\alpha \leq 1$  significantly increased compared to the identification accuracy of original feature vectors ( $P < 0.01$ , Tukey's HSD post-hoc test; Fig. 4a) and the identification accuracies corresponding to the brain-grounded vectors with  $\alpha = 10^{-2}$  and  $\alpha = 10^{-3}$  became significantly higher than identification accuracy corresponding to the vectors with  $\alpha = 1$  ( $P < 0.05$ , Tukey's HSD post-hoc test; Fig. 4c), while identification accuracies corresponding to the brain-grounded vectors with  $\alpha = 10^{-1}$  and  $\alpha = 10^{-4}$  became significantly lower than identification accuracy corresponding to the vectors with  $\alpha = 1$  ( $P < 0.05$ , Tukey's HSD post-hoc test; Fig. 4c)

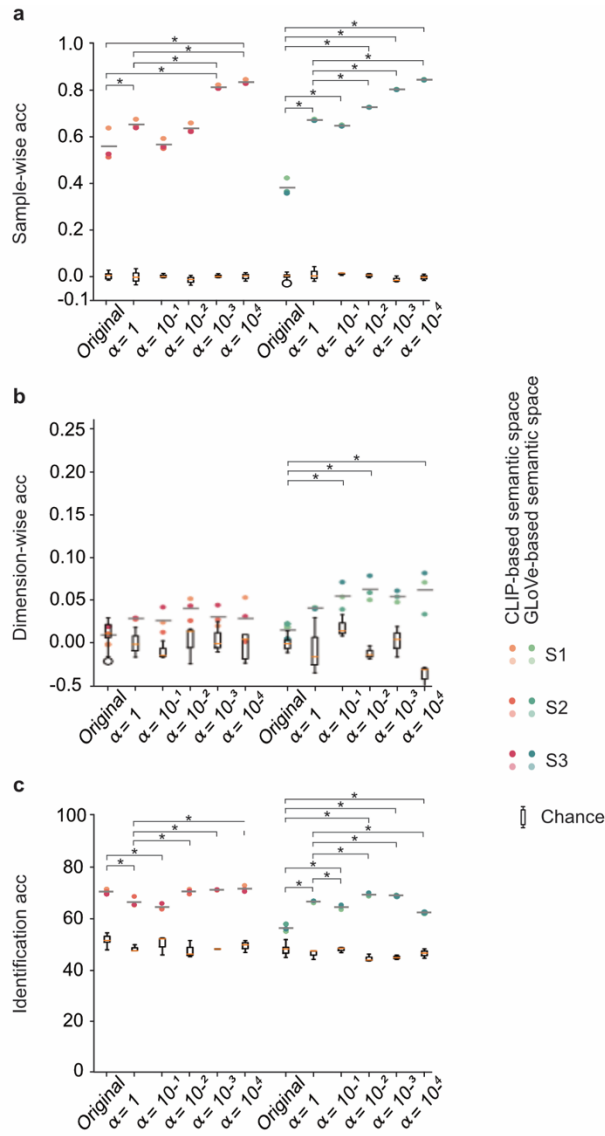


**Figure 4: Decoding and identification of perceptual content from MEG neural data.** Perceptual content is decoded and identified from MEG neural recordings, using original and brain-grounded feature vectors of CLIP and GloVe. Decoding accuracy is assessed by (a) sample-wise and (b) dimension-wise measurements. (c) depicts the MEG identification results. For clarity, only the significant differences between the brain-grounded vectors and with the original pretrained feature vectors and with the brain-grounded vectors with  $\alpha = 1$ , are depicted. For all results, see the supplementary figure 2.

Remarkably, in the ECoG results we observed that the sample-wise and dimension-wise decoding accuracy of brain-grounded vectors with  $\alpha = 10^{-4}$  were highest and increased to both original feature vectors and brain-grounded vectors with  $\alpha = 1$  (Fig 5a, b). Also, the identification accuracy of brain-grounded vectors with  $\alpha = 10^{-4}$  increased compared to the identification accuracy of original vectors for both CLIP-based and GloVe-based feature vectors (Fig 5c).

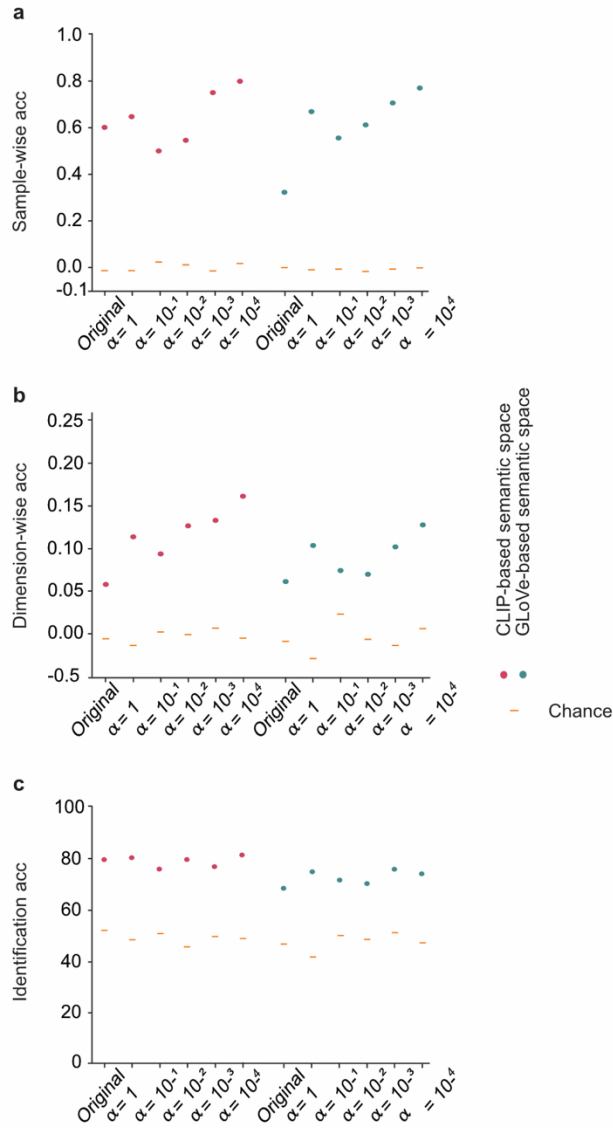


**Figure 5: Decoding and identification of perceptual content from ECoG neural recordings.** Visual stimuli are decoded and identified from ECoG recordings, using original and brain-grounded feature vectors of CLIP and GloVe. Decoding accuracy is assessed by (a) sample-wise and (b) dimension-wise measurements. (c) depicts the identification results. Dots representing the ECoG results indicates decoding/identification accuracy of concatenated subjects.

## Discussion

In this study, we demonstrated the ability of brain-grounding to enhance the zero-shot brain decoding across diverse neuroimaging datasets and subjects. Notably, fMRI brain decoders trained on the CLIP-based and GloVe-based brain-grounded feature vectors outperformed those trained on the original pretrained vectors, particularly when utilizing vectors with the highest level of brain alignment (brain-grounded vectors with  $\alpha = 10^{-4}$ ) (Fig 3a, b). Critically, this improvement was observed even for other types of neuroimaging neural data (MEG and ECoG), subjects, and stimulus categories that were not included in training the brain-grounding model (Fig 4a, b, and Fig 5a, b), highlighting the robustness and generalizability of our approach.



Furthermore, the brain-grounding process did not compromise identification accuracy in neither case, reinforcing the potential of this technique for real-world applications requiring both precise decoding and identification (Fig 3e, 3f, 4c and 5c).

The quest to create a brain-based semantic representation space has been explored in previous work. In a seminal study, Binder et al. (2016)<sup>45</sup> proposed a model where word meanings are represented as combinations of basic sensory, motor, affective, and cognitive experiences. They proposed a basic set of approximately 65 experiential attributes based on neurobiological considerations, comprising sensory, motor, spatial, temporal, affective, social, and cognitive experiences. They collected normative data on these experiential attributes to create a semantic space grounded in brain activity. Chersoni et al. (2021)<sup>46</sup> further advanced this concept by demonstrating the decoding of word embeddings using brain-based semantic features derived from fMRI data. However, while Binder et al. (2016) established a foundation for linking brain activity to semantic representations, their approach relied on hand-crafted attributes rather than directly utilizing the raw neural data. In contrast, our study harnesses the inherent structure of neural representations by directly leveraging the second-order statistical characteristics of brain activity patterns, avoiding the need for manual attribute definition. This data-driven approach may offer a more direct and potentially comprehensive representation of neural semantic space.

Besides creating brain-based semantic spaces, as exemplified by Binder et al. (2016), several studies have investigated fine-tuning neural representations with human's, monkeys' or rats' brain-based information to enhance performance on downstream tasks. For example, Federer et al. (2020)<sup>32</sup> showed that training neural networks to mimic the statistical properties of brain activity can improve object recognition. Li et al. (2024)<sup>47</sup> integrated deep neural network features with brain network information to enhance the prediction of brain activity during naturalistic perception. Muttenthaler et al. (2023)<sup>33</sup> explored aligning neural network representations with human similarity judgments to improve few-shot learning and anomaly detection. Additionally, Schneider et al. (2023)<sup>34</sup> demonstrated the power of combining behavioral and neural data through latent embeddings for predicting behavior. However, despite these advancements, previous research has not explicitly explored fine-tuning pretrained feature vectors to directly match the second-order statistical representations of human brain activity, nor have they systematically investigated the resulting zero-shot decoding performance on new subjects and neuroimaging modalities. Our brain-grounding method addresses this gap by aligning feature vector relationships with those observed in neural responses, demonstrating robust cross-modality and cross-subject decoding capabilities.

Our findings resonate with the broader literature on hyperalignment<sup>48</sup> and the quest to discover shared neural representational spaces across individuals. While our primary goal wasn't to derive a common high-dimensional space *per se*, our results nevertheless suggest a degree of alignment. By creating brain-grounded vectors based on averaged representational similarity matrices (RSMs) across subjects, we

effectively tapped into shared neural representations that transcend individual differences. The subsequent successful decoding of neural activity patterns from a different set of subjects aligns with studies like Guntupalli et al. (2016)<sup>49</sup> which demonstrated the feasibility of finding such shared spaces even at a fine-grained, searchlight level. Furthermore, our results extend this notion of shared representations across neuroimaging modalities, echoing findings from studies like Haxby et al. (2011)<sup>48</sup> that suggest the existence of common representational structures in fMRI data. Notably, in our study, the successful decoding of MEG and even ECoG signals using our fMRI-derived brain-grounded vectors provides evidence, for a shared representational space with consistent second-order statistical characteristics across these distinct modalities.

In conclusion, our study demonstrates the remarkable potential of brain-grounding semantic vectors to enhance the accuracy and generalizability of neural decoding algorithms. By integrating brain-like information into pretrained feature vectors, we achieved robust zero-shot decoding performance across different subjects and neuroimaging modalities, even with a relatively small fMRI dataset (approximately 150 categories). This suggests that our approach efficiently captures essential neural representations even with limited training data. While these results are promising, several avenues remain for future exploration. Investigating the impact of different autoencoder architectures, training strategies, loss metrics, and leveraging larger datasets could further optimize the effectiveness of brain-grounded vectors. Additionally, developing methods to mitigate potential biases in the brain-grounding process and enhance the interpretability of the resulting vectors would be valuable for their real-world application. Beyond these immediate refinements, future work could explore the application of brain-grounding to a broader range of cognitive domains and tasks, ultimately paving the way for more powerful and versatile brain-machine interface technologies.

## **Methods**

### **Creating semantic vectors**

Semantic vectors are multidimensional representations of data that encode the underlying semantics, relationships, and context within that data. In the context of brain decoding analysis, they have been widely used as a meaningful representation of stimuli to train decoders to learn to map neural activity patterns to their corresponding semantic vector representations. In this study, we used two different types of semantic spaces that have been previously used in brain decoding studies. Namely, we used pretrained feature vectors from the last layer of CLIP's image encoder and pretrained feature vectors from the GloVe model. We created semantic vectors for all categories in the ImageNet dataset fall 2011 release<sup>33</sup>.

#### *GloVe*

GloVe is a method that can generate 300-dimensional semantic vector representations of a given word, from a normalized version of statistical results of word co-occurrences obtained from a corpus consisting of more than 42 billion tokens. Words with similar meanings have vectors that are close in the vector space, enabling

GLoVe to capture the semantics of words and their contextual associations. Here we used the pretrained word vectors of the 42B tokens file (<https://nlp.stanford.edu/data/glove.42B.300d.zip>). For each image category in ImageNet dataset, we considered their annotations obtained by crowdsourcing of ImageNet dataset<sup>33</sup>, and calculated the averaged GLoVe representations of all available annotations in GloVe dictionary, as a representation of that category. If none of the annotations of a particular category didn't exist in GLoVe dictionary, that category was excluded from the whole analysis in this study.

### *CLIP*

CLIP is a model that connects vision and language by generating semantic vectors for both images and text. The unique strength of CLIP lies in its ability to map images and textual descriptions into a shared vector space, where the similarity or dissimilarity between vectors accurately reflects the semantic relationships between the two modalities. To create a CLIP semantic vector for each category in ImageNet, we extracted an image from each category, and then extracted the features from the ViT-B/32 Transformer image encoder of the CLIP model for each image.

## **fMRI dataset**

### *Dataset description*

We made use of one publicly available dataset, commonly referred as “Generic Object Decoding”<sup>18</sup>. Five healthy subjects (one female and four males, aged between 23 and 38 years) with normal or corrected-to-normal vision had participated in their experiments. Experiments consisted of presenting natural object images to subjects and recording their brain activity while they were perceiving the visual stimuli (perception experiment) or imagining them (imagery experiment). Images were selected from the ImageNet dataset. Training dataset consisted of neural recording of 1200 images (150 categories, 8 images per category), all performed in perception manner. Test dataset consisted of both perception and imagery neural recordings of 50 images (50 images were selected from 50 categories that were not used in the training dataset, 1 image per category, presented 35, 10 times respectively) and the study protocol was approved by the Ethics Committee of ATR. The LOC brain region was identified using the functional localizer experiment and SPM5 software.

## **MEG dataset**

### *MEG Experiment*

MEG experiments were conducted within our laboratory. Three subjects (3 males, aged between 25 and 34) were seeing images from the GOD dataset, while their brain activity was recorded with MEG. Experiments were conducted in perception manner. Each of the images in either training or test data was repeated 6 times and participants were asked to fixate on a central dot on images. The study adhered to the Declaration of Helsinki and was performed in accordance with the protocols approved by the ethics committee of our University Clinical Trial Center (No. 18472-5). All participants approved and signed the informed consent.

### *MEG preprocessing*

The process was initiated by importing the raw MEG data into Brainstorm<sup>41</sup>, a specialized software tool for neuroimaging analysis. Subsequently, essential filters were employed, including a high-pass filter at 0.5 Hz and a notch filter at 60Hz and its harmonics to eliminate unwanted frequency components. To address potential artifacts, Independent Component Analysis (ICA) was employed to extract cardiac and blink artifacts. The robustness of the analysis was further enhanced by utilizing room data to compute noise covariance and generating a subject-specific head model from individual MRI data. This enabled the accurate estimation of neural sources in the brain. Following source estimation, individual source activities were projected onto the default brain model (FSAverage) for consistency. To precisely mark the onset of each stimulus, analogue triggers were utilized. After these preprocessing steps, a high-quality dataset was obtained in the form of a matrix with dimensions of 200 samples (equivalent to milliseconds) by 7200 trials by 15002 vertices. Subsequently, the sensorimotor cortical potential (SCP), was calculated by averaging signals within specific time windows, resulting in a 7200 by 15002 matrix that served as the foundation for subsequent analyses.

#### *MEG ROI selection*

ROI selection consisted of two steps. First the neural sources in the brain that underlie the recorded MEG signals were estimated through a process called source localization<sup>42</sup>. These source localized data were then anatomically registered to the Human Connectome Project's HCP brain parcellation<sup>43</sup>. In our study, we selected the source localized data from the ventral visual cortex (VSVC). All the above-mentioned processes were performed using brainstorm.

### **ECoG dataset**

#### *Experimental settings*

The experiments were conducted with a cohort of epilepsy patients who had undergone neurosurgical procedures for the implantation of intracranial electrodes. These electrodes were intended to localize the epileptogenic zones responsible for seizure onset. During experiments, the subjects either sat on beds in their hospital rooms or were seated on chairs in front of a computer screen to watch the visual stimuli. The intracranial brain signals from each subject were recorded by EEG-1200 (Nihon Koden, Tokyo, Japan) with sampling rate of 10 kHz. Digital triggers encoding the presentation timing of the visual stimuli were generated by DATAPixx3 (VPixx Technologies, Quebec, Canada) and recorded synchronously with the ECoG signals. The study adhered to the Declaration of Helsinki and was performed in accordance with the protocols approved by the ethics committee of our University Clinical Trial Center (No. 14353). All participants approved and signed the informed consent.

#### *Experimental procedures*

Seventeen subjects participated in the image presentation task. These tasks were completed in 2 to 4 recording sessions over 1 to 3 days. To compensate for session-to-session changes in electrode impedance, baseline ECoG recordings were performed in a separate recording task, which was performed at the beginning of each recording session. Of the initial cohort, four subjects were selected for further analysis

based on two criteria: 1) the presence of electrodes implanted within their ventral visual cortex, and 2) demonstration of initial decoding performance exceeding chance levels. The number of electrodes in these four subjects were 74, 56, 30, and 71, respectively.

#### *Baseline recording task*

For the compensation of the session-to-session differences in electrode impedance, the baseline recording task was performed at the beginning of each recording session. The task consisted of one run, in which the subjects were presented with images from a baseline image dataset in random order without a blank screen between the presentations. The subjects were instructed to view the presented images while keeping their eyes on a red fixation point at the center of the screen. The duration of the presentation of each image was 1100ms.

#### *Image presentation task*

In the image presentation task, the GOD image dataset was presented to the subjects as a visual stimulus. Presentation of the GOD training images and evaluation images was performed in two and one runs, respectively, although the architecture of the runs was the same. Each subject participated in one or multiple training and evaluation runs. In each run, 10 images of the preceding stimuli image dataset were first presented in random order, followed by images from the GOD image dataset, which was also presented in random order. There were no blanks between the presentation of the images. The duration of the presentation of each image 500ms. During this task, the subjects were instructed to view the images with their eyes on the red fixation point in the center of the screen. The division of the GOD training images for the two runs was randomized for each pair of runs, and the corresponding runs in a pair were always performed in the same recording session.

#### *ECoG preprocessing*

For each subject, we performed a visual inspection of raw data and removed noisy channels. Common Average Referencing was then applied to mitigate common noise sources and accentuate local neural activity. ECoG epochs, time-locked to stimulus onset and extending 0.5 seconds post-stimulus, were extracted to focus on stimulus-related processing. Power Spectral Density (PSD) analysis was performed on each epoch, and high gamma power (80-150 Hz) was extracted as a feature of interest due to its established association with cognitive processes. These high gamma features subsequently served as input for statistical analyses investigating neural activity patterns in relation to experimental conditions. Finally, we concatenated the data corresponding to electrodes that were placed in the ventral visual stream of patients as the final ECoG data.

#### **Autoencoder framework**

The autoencoder consists of two fully connected layers with ReLU activation functions. The number of dimensions in the autoencoder's latent space is set to be half of the number of dimensions of the original vectors. For each subject, brain region and semantic space type, a separate autoencoder was trained. When training the autoencoder for a particular subject, we used the averaged brain RSMs of all other subjects.

After we could finish the training process, we fed all original semantic vectors to the trained model used the intermediate features of the resulting trained autoencoder as the brain-grounded features.

The RSM matrices were created from brain activity pattern or the autoencoder's latent space by calculating the pairwise cosine similarity of each of the two data points. During the training process, we used the difference between upper triangle of each of the RSM matrices to constrain the autoencoder to make representations to be more brain-like.

### Neural decoding of visual stimuli

We performed brain decoding by constructing linear regression models to predict semantic vectors from brain activity patterns. For predicting each unit of semantic vectors, a separate set of linear regression models were trained. Prior to applying regression analysis, we performed voxel selection similar to the method Horikawa et al. (2017) have used, and brain activity patterns were Z-normalized.

More formally, given brain activity patterns as  $x = \{x_1, x_2, \dots, x_n\}^T$  representing activity of  $n$  neural activity data points (i.e., voxels in the fMRI data, source estimated neural activity patterns from MEG sensors, neural amplitude recorded from each channel in each second in the ECoG) from the region of interest, regression function can be represented as:

$$y(x) = \sum_{i=1}^n w_i x_i + w_0$$

where  $x_i$  is a scalar value specifying amplitude of the brain data point  $i$ ,  $w_i$  is the weight of voxel  $i$  and  $w_0$  is the bias.

For each subject, semantic space type and brain region, we trained a separate set of linear regression function as decoders. When decoding fMRI data of a particular subject to the brain-grounded semantic spaces, we used the brain-grounded space in which that subject was not used to create. When decoding MEG data of a particular subject, we used the averaged brain-grounded semantic spaces of all fMRI subjects.

### Identification analysis

In the identification analysis, the predicted vector was identified among a large set of candidate vectors. First, we prepared one random image from each class of ImageNet dataset. Then, for each semantic space (i.e., GloVe and CLIP's pretrained feature vectors or GLoVe and CLIP's brain-grounded vectors for different values of  $\alpha$ ), we calculated the corresponding semantic vectors of all images that we had been randomly selected from the ImageNet. If we couldn't obtain the GLoVe embeddings of a category, that category was getting excluded from the whole analysis. When obtaining the brain-grounded vectors of all ImageNet categories, we fed the original GLoVe/CLIP pretrained feature vectors to the corresponding trained autoencoder and obtained the corresponding brain-grounded vectors. Then, for each category in the GOD dataset, we calculated the Pearson correlation coefficient of true and predicted vector, and the

predicted vector and all other candidate vectors, and assigned the identification accuracy as the percentage of candidate categories, in which their correlation with the test predicted vector was lower than the correlation of true and predicted vectors. Chance-level identification accuracy was determined by randomly shuffling the true feature vectors and calculating identification accuracy between the predicted and shuffled vectors, following the same procedure as for the unshuffled data.

### **Statistical test**

In the decoding analyses, we evaluated the performance of brain decoders using Pearson correlation coefficients between predicted and true feature vectors, as well as between the predicted and shuffled true feature vectors. Then, we applied Fisher's z-transform on the correlations of each case to stabilize variance, followed by one-sided t-tests for each feature space type and neuroimaging modality. Similarly in the identification analysis, we calculated the one-sided t-test between the identification results of shuffled data and unshuffled data.

To compare the decoding and identification accuracy means among the original feature vectors and brain-grounded feature vectors, we applied one-way analysis of variance (ANOVA) followed by Tukey's Honestly Significant Difference (HSD) post hoc test. Prior to each t-test and ANOVA, we assessed the normality of the data using the Shapiro-Wilk test.

To calculate the statistical differences of F-value distributions among different types of CLIP-based feature vectors (original or brain-grounded) we applied the two-sided Wilcoxon rank-sum test between each pairwise combination of original and/or brain-grounded feature vectors.

### **Acknowledgements**

We thank M. Abdelhack for help with introducing critical papers relevant to our study; R. Fukuma, T. Yanagisawa and K. Majima for help and advice with the methodology; R. Fukuma and H. Yang. for advice on MEG and ECoG data preprocessing; T. Yanagisawa for advice on statistical analysis; and R. Fukuma and T. Yanagisawa for comments on the manuscript and figures.

### **Author contributions**

S.V., R. F. and T.Y. conceptualized the project. S.V. was responsible for the theory. S.V., R.F. and T.Y. were responsible for the methodology. S.V. undertook the analysis and investigation. R. F., H. Y. were responsible for MEG and ECoG experiments. S.V. was responsible for data preprocessing and curation. S.V. wrote the original draft and created the figures. S.V. and T.Y edited the final version of the article.

### **Data and code availability**

should be addressed to Takufumi Yanagisawa.

## Competing interests

Authors declares no competing interests.

## References

1. Stavisky, S. D. & Wairagkar, M. Listening in to perceived speech with contrastive learning. *Nat. Mach. Intell.* (2023) doi:10.1038/s42256-023-00742-1.
2. Lebedev, M. A. & Nicolelis, M. A. L. Brain–machine interfaces: past, present and future. *Trends Neurosci.* **29**, 536–546 (2006).
3. Willett, F. R. *et al.* A high-performance speech neuroprosthesis. *Nature* **620**, 1031–1036 (2023).
4. Willsey, M. S. *et al.* Real-time brain-machine interface in non-human primates achieves high-velocity prosthetic finger movements using a shallow feedforward neural network decoder. *Nat. Commun.* **13**, 6899 (2022).
5. Haynes, J.-D. & Rees, G. Decoding mental states from brain activity in humans. *Nat. Rev. Neurosci.* **7**, 523–534 (2006).
6. Naselaris, T., Kay, K. N., Nishimoto, S. & Gallant, J. L. Encoding and decoding in fMRI. *Neuroimage* **56**, 400–410 (2011).
7. Haxby, J. V. *et al.* Distributed and Overlapping Representations of Faces and Objects in Ventral Temporal Cortex. *Science* **293**, 2425–2430 (2001).
8. Yamins, D. L. K. *et al.* Performance-optimized hierarchical models predict neural responses in higher visual cortex. *Proc. Natl. Acad. Sci.* **111**, 8619–8624 (2014).
9. Kellis, S. *et al.* Decoding spoken words using local field potentials recorded from the cortical surface. *J. Neural Eng.* **7**, 056007 (2010).
10. Brouwer, G. J. & Heeger, D. J. Decoding and Reconstructing Color from Responses in Human Visual Cortex. *J. Neurosci.* **29**, 13992–14003 (2009).
11. Sitaram, R. *et al.* Closed-loop brain training: the science of neurofeedback. *Nat. Rev. Neurosci.* **18**, 86–100 (2017).
12. Fukuma, R. *et al.* Voluntary control of semantic neural representations by imagery with conflicting visual stimulation. *Commun. Biol.* **5**, 214 (2022).
13. Chaudhary, U. *et al.* Spelling interface using intracortical signals in a completely locked-in patient enabled via auditory neurofeedback training. *Nat. Commun.* **13**, 1236 (2022).
14. Cortese, A., Amano, K., Koizumi, A., Kawato, M. & Lau, H. Multivoxel neurofeedback selectively modulates confidence without changing perceptual performance. *Nat. Commun.* **7**, 13669 (2016).
15. Horikawa, T. & Kamitani, Y. Generic decoding of seen and imagined objects using hierarchical visual features. *Nat. Commun.* **8**, 15037 (2017).
16. Haynes, J.-D. & Rees, G. Predicting the orientation of invisible stimuli from activity in human primary visual cortex. *Nat. Neurosci.* **8**, 686–691 (2005).
17. Kamitani, Y. & Tong, F. Decoding the visual and subjective contents of the human brain. *Nat. Neurosci.* **8**, 679–685 (2005).
18. Thirion, B. *et al.* Inverse retinotopy: Inferring the visual content of images from brain activation patterns. *NeuroImage* **33**, 1104–1116 (2006).
19. Cox, D. D. & Savoy, R. L. Functional magnetic resonance imaging (fMRI) “brain reading”: detecting and classifying distributed patterns of fMRI activity in human visual cortex. *NeuroImage* **19**, 261–270 (2003).
20. Nakai, T., Koide-Majima, N. & Nishimoto, S. Correspondence of categorical and feature-based representations of music in the human brain. *Brain Behav.* **11**, e01936 (2021).
21. Koide-Majima, N., Nishimoto, S. & Majima, K. Mental image reconstruction from human brain activity. *bioRxiv* (2023) doi:10.1101/2023.01.22.525062.
22. Miyawaki, Y. *et al.* Visual image reconstruction from human brain activity using a combination of multiscale local image decoders. *Neuron* **60**, 915–929 (2008).



23. Shen, G., Dwivedi, K., Majima, K., Horikawa, T. & Kamitani, Y. End-to-End Deep Image Reconstruction From Human Brain Activity. *Front. Comput. Neurosci.* **13**, (2019).
24. Shen, G., Horikawa, T., Majima, K. & Kamitani, Y. Deep image reconstruction from human brain activity. *PLoS Comput. Biol.* **15**, e1006633 (2019).
25. Krizhevsky, A., Sutskever, I. & Hinton, G. E. ImageNet Classification with Deep Convolutional Neural Networks. in *Advances in Neural Information Processing Systems* (eds. Pereira, F., Burges, C. J., Bottou, L. & Weinberger, K. Q.) vol. 25 (Curran Associates, Inc., 2012).
26. Liu, Y., Ma, Y., Zhou, W., Zhu, G. & Zheng, N. BrainCLIP: Bridging Brain and Visual-Linguistic Representation Via CLIP for Generic Natural Visual Stimulus Decoding. *ArXiv Prepr. ArXiv230212971* (2023).
27. Radford, A. *et al.* Learning transferable visual models from natural language supervision. in 8748–8763 (PMLR, 2021).
28. Pereira, F. *et al.* Toward a universal decoder of linguistic meaning from brain activation. *Nat. Commun.* **9**, 963 (2018).
29. Mikolov, T., Chen, K., Corrado, G. S. & Dean, J. Efficient Estimation of Word Representations in Vector Space. in *International Conference on Learning Representations* (2013).
30. Pennington, J., Socher, R. & Manning, C. GloVe: Global Vectors for Word Representation. in *Proceedings of the 2014 Conference on Empirical Methods in Natural Language Processing (EMNLP)* 1532–1543 (Association for Computational Linguistics, Doha, Qatar, 2014). doi:10.3115/v1/D14-1162.
31. Shirakawa, K. *et al.* Spurious reconstruction from brain activity. *ArXiv Prepr. ArXiv240510078* (2024).
32. Federer, C., Xu, H., Fyshe, A. & Zylberberg, J. Improved object recognition using neural networks trained to mimic the brain's statistical properties. *Neural Netw.* **131**, 103–114 (2020).
33. Muttenthaler, L. *et al.* Improving neural network representations using human similarity judgments. *ArXiv Prepr. ArXiv230604507* (2023).
34. Schneider, S., Lee, J. H. & Mathis, M. W. Learnable latent embeddings for joint behavioural and neural analysis. *Nature* **617**, 360–368 (2023).
35. Kay, K. N., Naselaris, T., Prenger, R. J. & Gallant, J. L. Identifying natural images from human brain activity. *Nature* **452**, 352–355 (2008).
36. Ogawa, S., Lee, T.-M., Kay, A. R. & Tank, D. W. Brain magnetic resonance imaging with contrast dependent on blood oxygenation. *Proc. Natl. Acad. Sci.* **87**, 9868–9872 (1990).
37. Penfield, W. & Jasper, H. Epilepsy and the functional anatomy of the human brain. (1954).
38. Cohen, D. Magnetoencephalography: evidence of magnetic fields produced by alpha-rhythm currents. *Science* **161**, 784–786 (1968).
39. Deng, J. *et al.* ImageNet: A large-scale hierarchical image database. in *2009 IEEE Conference on Computer Vision and Pattern Recognition* 248–255 (2009). doi:10.1109/CVPR.2009.5206848.
40. Kourtzi, Z. & Kanwisher, N. Cortical Regions Involved in Perceiving Object Shape. *J. Neurosci.* **20**, 3310–3318 (2000).
41. Norman, K. A., Polyn, S. M., Detre, G. J. & Haxby, J. V. Beyond mind-reading: multi-voxel pattern analysis of fMRI data. *Trends Cogn. Sci.* **10**, 424–430 (2006).
42. Cichy, R. M., Pantazis, D. & Oliva, A. Resolving human object recognition in space and time. *Nat. Neurosci.* **17**, 455–462 (2014).
43. Horikawa, T., Tamaki, M., Miyawaki, Y. & Kamitani, Y. Neural decoding of visual imagery during sleep. *Science* **340**, 639–642 (2013).
44. Mitchell, T. M. *et al.* Predicting human brain activity associated with the meanings of nouns. *science* **320**, 1191–1195 (2008).
45. Binder, J. R. *et al.* Toward a brain-based componential semantic representation. *Cogn. Neuropsychol.* **33**, 130–174 (2016).
46. Chersoni, E., Santus, E., Huang, C.-R. & Lenci, A. Decoding Word Embeddings with Brain-Based Semantic Features. *Comput. Linguist.* **47**, 663–698 (2021).
47. Li, Y., Yang, H. & Gu, S. Enhancing neural encoding models for naturalistic perception with a multi-level integration of deep neural networks and cortical networks. *Sci. Bull.* (2024) doi:https://doi.org/10.1016/j.scib.2024.02.035.
48. Haxby, J. V. *et al.* A common, high-dimensional model of the representational space in human ventral temporal cortex. *Neuron* **72**, 404–416 (2011).

49. Guntupalli, J. S. *et al.* A model of representational spaces in human cortex. *Cereb. Cortex* **26**, 2919–2934 (2016).